Journal of Renewable Materials

Tech Science Press

DOI: 10.32604/jrm.2023.025241

ARTICLE

Optimization of Preparation of Fe_3O_4-L by Chemical Co-Precipitation and Its Adsorption of Heavy Metal Ions

Junzhen Di, Xueying Sun*, Siyi Zhang, Yanrong Dong and Bofu Yuan

College of Civil Engineering, Liaoning Technical University, Fuxin, 123000, China

*Corresponding Author: Xueying Sun. Email: sunxueyingup@126.com

Received: 30 June 2022 Accepted: 16 August 2022

ABSTRACT

To address the serious pollution of heavy metals in AMD, the difficulty and the high cost of treatment, Fe_3O_4-L was prepared by the chemical co-precipitation method. Based on the single-factor and RSM, the effects of particle size, total Fe concentration, the molar ratio of Fe^{2+} to Fe^{3+} and water bath temperature on the removal of AMD by Fe_3O_4-L prepared by chemical co-precipitation method were analyzed. Static adsorption experiments were conducted on Cu^{2+}, Zn^{2+} and Pb^{2+} using Fe_3O_4-L prepared under optimal conditions as adsorbents. The adsorption properties and mechanisms were analyzed by combining SEM-EDS, XRD and FTIR for characterization. The study showed that the effects of particle size, total Fe concentration and the molar ratio of Fe^{2+} to Fe^{3+} are larger. Obtained by response surface optimization analysis, the optimum conditions for the preparation of Fe_3O_4-L were a particle size of 250 mesh, a total Fe concentration of 0.5 mol/L, and a molar ratio of Fe^{2+} to Fe^{3+} of 1:2. Under these conditions, the removal rates of Cu^{2+}, Zn^{2+}, and Pb^{2+} were 94.52%, 88.49%, and 96.69% respectively. The adsorption of Cu^{2+}, Zn^{2+} and Pb^{2+} by Fe_3O_4-L prepared under optimal conditions reached equilibrium at 180 min, with removal rates of 99.99%, 85.27%, and 97.48%, respectively. The adsorption reaction of Fe_3O_4-L for Cu^{2+} and Zn^{2+} is endothermic, while that for Pb^{2+} is exothermic. Fe_3O_4-L can still maintain a high adsorption capacity after five cycles of adsorption-desorption experiments. Cu^{2+}, Zn^{2+} and Pb^{2+} mainly exist as $CuFe_2O_4$, $Zn(OH)_2$, $ZnFe_2O_4$ and PbS after being adsorbed by Fe_3O_4-L, which is the result of the combination of physical diffusion, ion exchange and surface complexation reaction.

KEYWORDS

Chemical co-precipitation; Fe_3O_4-L; single-factor experiment; RSM; adsorption; characterization

1 Introduction

With the increasing demand for industrial society development and the increasing use of mineral resources, Acid Mine Drainage (AMD) from coal mining has increased dramatically. AMD is characterized by low pH and high heavy metal ion content. The heavy metal ions such as Cu^{2+}, Zn^{2+} and Pb^{2+} have a continuous and cumulative impact on the environment. If improperly treated and discharged, they will seriously pollute waters and negatively affect the ecological environment [1,2]. The adsorption method is widely used in the treatment of AMD because of its simple design, easy operation and high economic efficiency [3]. The choice of adsorbent is very important when using the adsorption method to

treat AMD. Thus, the cost, adsorption capacity and post-use recycling of it should be reasonably considered when selecting the adsorbent [4].

Common natural adsorbents include activated carbon, zeolite, bentonite and lignite, etc. Yin et al. [5] designed response surface experiments to optimize the preparation and adsorption conditions of activated carbon. The optimum preparation conditions of impregnation ratio, activation time and activation temperature were 2.3, 100 min and 510°C, respectively, and the optimum adsorption capacity for Pb^{2+} was 42.85 mg/g. Activated carbon performs poorly in treating wastewater containing heavy metal ions, so a chelating agent is needed to improve its performance, which will greatly increase the cost [3]. Lu et al. [3] proposed in a study on the adsorption and thermal stability of zeolites on Pb^{2+} and Cu^{2+} that zeolites are inexpensive and porous media that facilitate effective removal of heavy metal ions, but so far the problem of treatment of second-hand zeolite dealing with heavy metal ions has not been solved. Karapinar et al. [6] studied the adsorption behavior of natural bentonite for Cd^{2+} and Cu^{2+}, and carried out thermodynamic analysis under the optimized conditions. The results show that natural bentonite can effectively adsorb Cd^{2+} and Cu^{2+} from an aqueous solution. Olu-Owolabi et al. [7] modified bentonite with sulfate and phosphate to enhance the ion exchange capacity and improve the adsorption of Zn^{2+} and Cu^{2+}. Bentonite can effectively adsorb heavy metal ions, but powdered bentonite will be mixed into mud when put into AMD, which is difficult to separate and recover. Lignite has the advantage of wide sources and low prices due to its large reserves and lower market prices than other coal-based fuels [8,9]. Lignite is considered as a good adsorbent because of its low density, large specific surface area and a large number of active groups that can chelate and complex with heavy metal ions. Chu et al. [10] studied the adsorption effect of lignite for Hg and As with kinetic fitting, and the results showed that the adsorption capacities of lignite for Hg and As were 6.8995 and 7.3995 mg/g, respectively, and the SEM characterization analysis showed that the pore structure of lignite was favorable for the adsorption of Hg and As. However, Di et al. [11] investigated the adsorption effect of native lignite and NaCl-modified lignite on Fe^{2+} and Mn^{2+}, respectively, and the results showed that the adsorption effect of unmodified lignite on Fe^{2+} and Mn^{2+} was average, while the removal rates of Fe^{2+} and Mn^{2+} by NaCl-modified lignite was significantly increased by 28.44% and 22.47% compared with that of unmodified lignite. Therefore, in order to achieve the desired effect, modification of the native lignite is required [12,13]. There are many ways to modify lignite, and considering the recycling problem, we have to find a modification method that is easy to separate after adsorption [1]. Magnetic modification technology can effectively improve the adsorption effect of materials, and the separated lignite can be reused after desorption and regeneration. The preparation methods of magnetic modified materials mainly include the co-precipitation method and the hydrothermal method [14–16]. Mahmud et al. [17] compared the properties of Fe_3O_4 particles prepared by chemical co-precipitation and hydrothermal methods. The particle size and thermal stability of Fe_3O_4 particles prepared by two methods were studied by particle size analysis and thermogravimetric analysis. The results showed that Fe_3O_4 particles with small particle size and high thermal stability can be more easily obtained by chemical co-precipitation method. The chemical co-precipitation method is to prepare magnetic materials by mixing Fe^{2+} and Fe^{3+} iron salts in an alkaline aqueous medium [18]. The method can obtain Fe_3O_4 particles with better quality, higher yield and controllable performance according to different chemical environments without the need for special chemicals and complex and harmful procedures [15,19–21]. Therefore, the chemical co-precipitation method is the most suitable, the most widely used and the most promising method to synthesize Fe_3O_4 particles [22].

In this paper, Fe_3O_4-loaded lignite (Fe_3O_4-L) was prepared based on chemical co-precipitation method. The effect of Fe_3O_4-L prepared under different reaction conditions on the removal of Cu^{2+}, Zn^{2+} and Pb^{2+} from AMD was investigated by single-factor experiments, and the factors with greater influence were analyzed and screened. The optimal preparation conditions of Fe_3O_4-L were optimized by response surface methodology (RSM). Static adsorption experiments were conducted on Cu^{2+}, Zn^{2+} and Pb^{2+}

using Fe_3O_4-L prepared under optimal conditions as adsorbent to obtain the removal rate laws for Fe_3O_4-L on Cu^{2+}, Zn^{2+} and Pb^{2+} at different initial concentrations for each temperature system and at different reaction times, and to investigate the effect of optimized Fe_3O_4-L for adsorption on Cu^{2+}, Zn^{2+} and Pb^{2+}. The lignite before and after modification and Fe_3O_4-L before and after adsorption were characterized by SEM-EDS, XRD and FTIR, and the mechanism of Fe_3O_4-L adsorption of Cu^{2+}, Zn^{2+} and Pb^{2+} was explored.

2 Materials and Methods

2.1 Experimental Materials and Water Samples

The lignite from Shanxi Fuhong Mineral Products Co., Ltd. (China) is crushed and passed through 150 mesh, 200 mesh and 250 mesh sieves respectively, deionized water is washed 2–3 times and then dried at 80°C. 200 mL iron solution with a total iron concentration of 0.7 mol/L was prepared according to the Fe^{2+} to Fe^{3+} molar ratio of 1:2 and heated in a constant temperature water bath at 60°C. 10 g of lignite was added into the iron solution and stirred at 350 r/min for 1 h. The concentrated ammonia water with a mass fraction of 25% was added drop by drop to a pH value of 9, continued stirring for 1 h, and then stood for 2 h. The precipitate was cleaned with deionized water, separated from solid and liquid by a rubidium magnet, repeatedly cleaned to the supernatant as neutral, dried in a vacuum for 12 h, and taken out. The sample solutions were prepared with analytically pure $FeSO_4{\cdot}7H_2O$, $Fe_2(SO_4)_3$, $CuSO_4{\cdot}5H_2O$, $ZnSO_4{\cdot}7H_2O$, $Pb(NO_3)_2$ and NaOH. The concentration of the sample solution was prepared according to the actual AMD water quality parameters in a mining area in Huludao: Cu^{2+} concentration was 30 mg/L, Zn^{2+} concentration was 30 mg/L, Pb^{2+} concentration was 50 mg/L, and pH was 4.

2.2 Detection Indicators and Methods

In this experiment, the concentrations of Cu^{2+}, Zn^{2+} and Pb^{2+} were measured by a Z-2000 flame atomic spectrophotometer (GB/T 7475-2015), and the pH was measured by PHS-3C pH meter through the glass electrode method (GB/T 6920-2015).

3 Experimental Design

3.1 Single-Factor Experiments

Previous studies have shown that the main influencing factors for the preparation of Fe_3O_4 particles by chemical co-precipitation are particle size, the ratio of Fe^{2+} to Fe^{3+} species, total iron concentration, water bath temperature, type of precipitant and pH [22,23]. When Fe_3O_4 particles are prepared by chemical co-precipitation, Fe^{2+} can be completely precipitated only when the pH reaches 8.9. Therefore, the preparation of Fe_3O_4 particles by chemical co-precipitation method needs to add an alkaline precipitant to adjust the pH [24]. Common precipitants include NaOH and $NH_3{\cdot}H_2O$. NaOH is a strong base and has a high alkali concentration of $-OH$, which is beneficial to the growth of the cell nucleus and can improve the speed of a chemical reaction, but the particle size of the generated Fe_3O_4 particles grows too fast and is prone to agglomeration [24,25]. $NH_3{\cdot}H_2O$ is a weak base, and its reaction rate is slightly slower than that of NaOH, which can better control the particle size of Fe_3O_4. Generally, $NH_3{\cdot}H_2O$ is used as the precipitant. A large number of research results show that pH will have a certain influence on the magnetic properties of Fe_3O_4 particles. When the pH value is 9, the prepared Fe_3O_4 particles have the best magnetic properties [24,26]. For lignite: the active ingredient HA in lignite will continuously dissolve under low alkalinity, which is beneficial to adsorption. However, HA will be degraded into small molecules under strong alkalinity, which reduces the chelating ability of metal ions and affects the inhibitory effect of HA on the release of metals in adsorption products [27,28]. Therefore, in this study, $NH_3{\cdot}H_2O$ was chosen as the precipitant to prepare Fe_3O_4-L under the condition of $pH = 9$.

Fe_3O_4-L is prepared by loading Fe_3O_4 particles on the lignite matrix. The performance of Fe_3O_4-L is affected by the loading capacity of lignite and the properties of Fe_3O_4 particles. The particle size of

lignite is different, the surface area is different, and the loading amount of Fe_3O_4 particles on the lignite surface is also different. Therefore, the particle size of lignite should be discussed as a single factor of preparation conditions. When Fe_3O_4 particles are prepared by chemical co-precipitation, the particle size and magnetic properties of Fe_3O_4 particles can be strictly controlled by changing the reaction temperature [23]. The desired magnetization and nanoparticle size can be achieved by adjusting the concentration of iron salts in the solution and the molar ratio of Fe^{2+} to Fe^{3+} [22,24]. Therefore, the ratio of the amount of Fe^{2+} to Fe^{3+}, the total iron concentration, and the temperature of the water bath should also be considered as single factors of the preparation conditions.

In order to prepare Fe_3O_4-L adsorption materials with excellent performance, $NH_3{\cdot}H_2O$ was chosen as the precipitant in this study, and the preparation conditions were explored under the condition of pH = 9. A single-factor experimental method was used to investigate the effects of particle size, the molar ratio of Fe^{2+} to Fe^{3+}, total Fe concentration and water bath temperature on the removal performance of Cu^{2+}, Zn^{2+} and Pb^{2+} under a single metal system in AMD-treated with Fe_3O_4-L.

Effect of particle size: Fe_3O_4-L was prepared in a constant temperature water bath at 60°C in the molar ratio of Fe^{2+} to Fe^{3+} of 1:2 and a total Fe concentration of 0.7 mol/L. The prepared Fe_3O_4-L was crushed and screened to 150 mesh, 200 mesh and 250 mesh. A 250 mL, pH = 4 solutions containing 30 mg/L Cu^{2+}, 30 mg/L Zn^{2+}, and 50 mg/L Pb^{2+} were prepared, respectively. 1.0 g of 150-mesh, 200-mesh, and 250-mesh Fe_3O_4-L were weighed and added to Cu^{2+}, Zn^{2+} and Pb^{2+} solutions, respectively. Three replicates of each experiment were made. The adsorption was shaken at 150 r/min and samples were collected every 30 min to detect the concentrations of Cu^{2+}, Zn^{2+} and Pb^{2+} in different Fe_3O_4-L particle size systems.

The following experimental procedures for the preparation of Fe_3O_4-L to remove Cu^{2+}, Zn^{2+} and Pb^{2+} are the same as the above experiments except that the materials of Fe_3O_4-L are different. Effect of the molar ratio of Fe^{2+} to Fe^{3+}: The Fe_3O_4-L with 250 mesh particle size was prepared in a constant temperature water bath at 60°C according to the molar ratio of Fe^{2+} to Fe^{3+} of 1:1, 1:1.5 and 1:2, respectively, and the total Fe concentration of 0.7 mol/L. Effect of total Fe concentration: The Fe_3O_4-L with a particle size of 250 mesh was prepared in a constant temperature water bath at 60°C according to the molar ratio of Fe^{2+} to Fe^{3+} of 1:2 and the total iron concentration of 0.5, 0.7 and 0.9 mol/L, respectively. Effect of water bath temperature: The Fe_3O_4-L with a particle size of 250 mesh was prepared in a constant temperature water bath of 50°C, 60°C and 70°C with the molar ratio of Fe^{2+} to Fe^{3+} of 1:2 and the total Fe concentration as 0.7 mol/L, respectively.

3.2 Response Surface Experiments

In this study, the Box-Benhnken method (BBD) was used to design response surface experiments using the results of single-factor experiments. Three independent variables, particle size (A), total Fe concentration (B) and the molar ratio of Fe^{2+} to Fe^{3+} (C), were used as response factors, which were varied at low (−1), medium (0) and high (1) levels, respectively, and the removal rates of Cu^{2+}, Zn^{2+} and Pb^{2+} from the experimental sample solutions were used as response values (Y) to design 17 sets of experiments. The response experimental design scheme and the results are given in Table 1. The second-order polynomial model was fitted using Design-Expert software, as in Eq. (1), to obtain the regression equation. Statistical significance of the model was assessed by analysis of variance (ANOVA), and variable interaction effects were analyzed using response surface plots [5,24].

$$Y = \beta_0 + \sum_{i=1}^{k} \beta_i X_i + \sum_{i=1}^{k} \beta_{ii} X_i^2 + \sum_{i=1}^{k-1} \sum_{j=}^{k} \beta_{ij} X_i X_j + \varepsilon \quad (1)$$

where, Y is the system response value; β_0 is the offset factor of the offset term; β_i is the linear offset coefficient; β_{ii} is the second-order offset coefficient; β_{ij} is the interaction effect coefficient; X_i, X_j and X_iX_j are the main and interaction effects of each factor for each factor level value analysis [29].

Table 1: Response surface test results

No.	Variable						Response value			Predicted value		
	Actual value			Code value								
	A	B	C	A	B	C	Cu^{2+}(%)	Zn^{2+}(%)	Pb^{2+}(%)	Cu^{2+}(%)	Zn^{2+}(%)	Pb^{2+}(%)
1	200	0.7	1:1.5	0	0	0	87.96	82.19	91.64	88.45	82.50	92.12
2	200	0.7	1:1.5	0	0	0	87.96	82.19	92.24	88.47	82.52	92.12
3	200	0.7	1:1.5	0	0	0	87.96	82.19	92.14	88.47	82.52	92.12
4	150	0.7	1:2	−1	0	1	85.24	76.62	82.14	85.91	76.18	82.93
5	250	0.7	1:1	1	0	−1	87.81	84.26	89.54	84.85	75.88	84.78
6	200	0.9	1:1	0	1	−1	84.85	83.02	87.54	85.14	82.97	88.35
7	250	0.7	1:2	1	0	1	93.09	86.36	91.84	93.51	86.72	92.70
8	150	0.9	1:1.5	−1	1	0	85.28	75.04	85.14	85.81	75.65	85.04
9	200	0.5	1:1	0	−1	−1	86.16	84.43	93.64	86.94	84.19	94.47
10	250	0.9	1:1.5	1	1	0	88.52	84.67	88.94	90.14	84.76	89.69
11	200	0.7	1:1.5	0	0	0	87.96	82.19	91.54	88.45	82.50	92.12
12	150	0.5	1:1.5	−1	−1	0	85.34	75.43	86.54	85.29	75.96	85.90
13	200	0.5	1:2	0	−1	1	90.39	85.29	94.74	89.99	85.34	93.93
14	200	0.7	1:1.5	0	0	0	87.96	82.19	92.74	88.45	82.50	92.12
15	250	0.5	1:1.5	1	−1	0	91.51	86.76	96.64	92.55	86.77	96.86
16	150	0.7	1:1	−1	0	−1	85.27	76.24	85.64	85.91	76.18	82.93
17	200	0.9	1:2	0	1	1	90.23	84.29	91.84	89.43	84.33	91.00

3.3 Adsorption of Cu^{2+}, Zn^{2+} and Pb^{2+} by Fe_3O_4-L

Fe_3O_4-L was prepared for the adsorption of Pb^{2+}, Cu^{2+}, and Zn^{2+} according to the optimal results of RSM. To investigate the adsorption effect of Fe_3O_4-L at different reaction times, 1.0 g Fe_3O_4-L was injected into the solutions of Cu^{2+} (30 mg/L), Zn^{2+} (30 mg/L) and Pb^{2+} (50 mg/L) at pH = 4, respectively. Adsorption by shaking at 150 r/min. The remaining ion concentrations were measured at 5, 10, 15, 30, 45, 60, 90, 120, 150 and 180 min. Each experiment was repeated three times. To investigate the removal effect of Fe_3O_4-L on metal ions at different initial concentrations in different temperature systems, 1.0 g Fe_3O_4-L was added to different concentrations of Cu^{2+} solution (10, 20, 30, 40, 50 mg/L), Zn^{2+} solution (10, 20, 30, 40, 50 mg/L) at pH = 4, and Pb^{2+} solution (10, 20, 30, 50, 70 mg/L) at pH = 4. The adsorption was carried out at temperatures of 25°C, 35°C and 45°C, respectively, for 180 min at an oscillation speed of 150 r/min. Each experiment was repeated three times. The residual Cu^{2+}, Zn^{2+} and Pb^{2+} concentrations were detected at different initial concentrations in different temperature systems.

In order to explore the reusability of Fe_3O_4-L, adsorption-desorption cycle experiments were carried out. Add 1.0 g Fe_3O_4-L to Cu^{2+} (30 mg/L), Zn^{2+} (30 mg/L), and Pb^{2+} (50 mg/L) solutions at pH = 4, and shake at 150 r/min for 180 min at 25°C. The remaining Cu^{2+}, Zn^{2+}, and Pb^{2+} concentrations in the supernatant were detected. Then, Fe_3O_4-L after adsorption of Cu^{2+}, Zn^{2+}, and Pb^{2+} was added to 250 mL of 0.1 mol/L HNO_3 and desorbed by shaking at 150 r/min for 180 min at 25°C to achieve the desorption of Cu^{2+}, Zn^{2+}, and Pb^{2+}. The desorbed Fe_3O_4-L was washed with deionized water until neutral, dried under vacuum for 12 h, and the above adsorption-desorption process was repeated five times. Each group of experiments was repeated three times.

3.4 Characterization

A scanning electron microscope (JSM-7610Plus, Japan) was used to observe the surface morphology of lignite as well as Fe_3O_4-L. The lignite and Fe_3O_4-L adsorbent before and after adsorption of metal ions were analyzed for elemental composition testing using an UltraDry EDS detector (Thermo ScientificTM, USA). The changes in the composition and surface functional groups of Fe_3O_4-L adsorbent before and after modification and adsorption were determined by an X-ray diffractometer (Shimadzu XRD-6100, Japan) and Fourier transform infrared spectrometer (Thermo Fisher Scientific IS10, USA).

4 Results and Analysis

4.1 Analysis of Single-Factor Experimental Results

The removal rates of Cu^{2+}, Zn^{2+} and Pb^{2+} by the prepared Fe_3O_4-L gradually rise with the increase of the particle size mesh (Figs. 1a–1c). The growth in particle size leads to an increase in the specific surface area and porosity of Fe_3O_4-L particles, which leads to an increase in the adsorption activity sites and facilitates the adsorption reaction.

The removal rates of Cu^{2+}, Zn^{2+} and Pb^{2+} by Fe_3O_4-L gradually increase as the ratio of Fe^{2+} to Fe^{3+} substance decreases (Figs. 1d–1f). The Fe^{3+} content affects the purity and porosity of Fe_3O_4-L. When the Fe^{3+} content in the solution is low, the prepared Fe_3O_4-L has more impurities and low purity. In the process of loading Fe_3O_4, the dissolution of Fe^{3+} will lead to the increase of H^+ content in the solution, resulting in the decomposition of some components of lignite that can produce new pore channels and increase the surface area and porosity [15,23,30]. The content of Fe^{2+} affects the Fe_3O_4 nanocrystal properties and yields. The increase of Fe^{2+} facilitates the reaction to produce Fe_3O_4 nanocrystals with larger particle size and better crystallinity, but the low yield leads to the reduction of Fe_3O_4 particles loaded on the surface of lignite, which affects the adsorption performance [23,24,30].

The removal rates of Cu^{2+}, Zn^{2+} and Pb^{2+} by Fe_3O_4-L show an increasing and then decreasing trend with the increase of total Fe concentration (Figs. 1g–1i). The total concentration of iron salts affects the crystallization of Fe_3O_4 nanoparticles. The process of preparing nanoparticles by chemical co-precipitation is divided into two stages: the crystal nucleation stage and the grain growth stage [31]. The iron salt concentration is low mainly in the nucleation stage, generating a large number of nuclei. However, the particle size of the product at this time is small, and the adsorption effect of Fe_3O_4-L is minimal. With the increase of iron salt concentration, the grain growth stage is entered. The grain growth rate is accelerated, the product particle size, surface area and porosity increase, and the adsorption capacity is strong. The total concentration of iron salts is getting higher and higher, and the iron salts react rapidly to generate nuclei after adding precipitant and grow continuously, with a large specific surface area and more adsorption sites. However, when the concentration is already too high, the generated Fe_3O_4 agglomerates seriously, and the pores of Fe_3O_4-L are gradually blocked, which affects the adsorption effect [32].

The removal of all three metal ions by Fe_3O_4-L increases with increasing reaction temperature, but then decreases when the temperature is too high (Figs. 1j–1l). The higher the reaction temperature, the greater the crystal growth rate and the larger the product particle size, which provides more adsorption sites and facilitates adsorption. However, the higher temperature tends to lead to crystal aggregation and blockage of Fe_3O_4-L pores, which is not conducive to adsorption [31]. Temperature affects the purity of Fe_3O_4-L. When the temperature increases, Fe^{2+} is easily oxidized to Fe^{3+}, and it is difficult to control the molar ratio of Fe^{2+} to Fe^{3+}, which leads to the increase of impurities in the product and reduces the adsorption capacity. Temperature affects the stability of Fe_3O_4 particles and thus the rate of their production. At lower temperatures, the solute energy is weak and the crystal formation rate is slow. As the temperature increases, the rate of crystal formation gradually reaches its maximum. The continued increase in temperature will cause the kinetic energy of molecules in solution to increase too fast, which is not conducive to the formation of stable particles and reduces the rate of crystal formation [33].

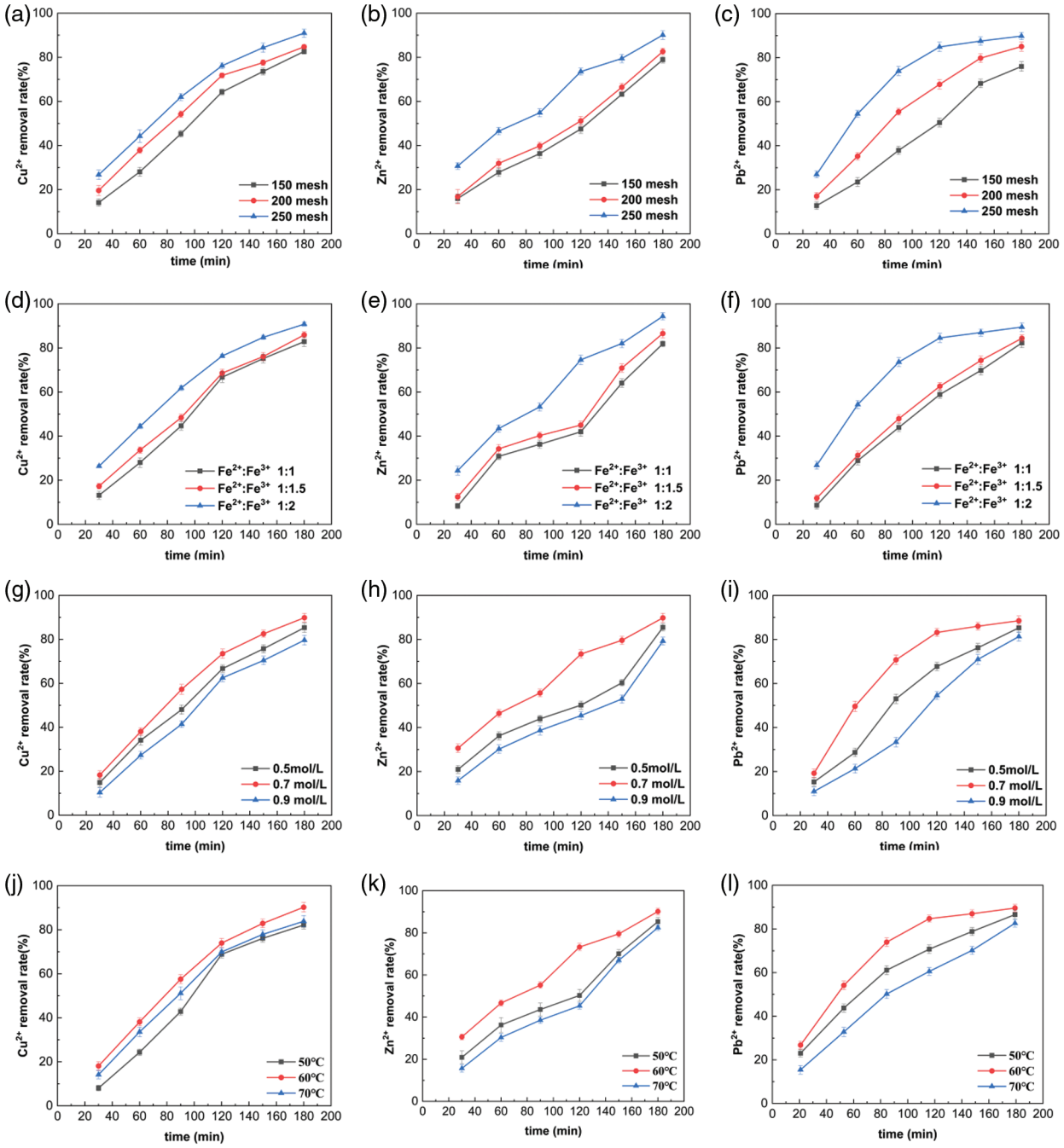

Figure 1: Effect of preparation conditions of Fe_3O_4-L on the removal of Cu^{2+}, Zn^{2+} and Pb^{2+}. (a–c) Particle size (Fe^{2+}:Fe^{3+}=1:2, total iron concentration = 0.7 mol/L, water bath temperature = 60°C) (d–f) Molar ratio of Fe^{2+} to Fe^{3+} (Particle size = 250 mesh, total iron concentration = 0.7 mol/L, water bath temperature = 60°C) (g–i) Total Fe concentration (Particle size = 250 mesh, Fe^{2+}:Fe^{3+} = 1:2, water bath temperature = 60°C) (k–l) Water bath temperature (Particle size = 250 mesh, Fe^{2+}:Fe^{3+} = 1:2, total iron concentration = 0.7 mol/L)

4.2 Analysis of Response Surface Experimental Results

ANOVA was used to assess the adequacy of the second-order regression model developed by BBD, and the results were shown in Tables 2–4. The F value and *P*-value of the model (Prob > F) determined the model significance. The model F values for Cu^{2+}, Zn^{2+}, and Pb^{2+} were 48.90, 137.74, and 27.31, respectively. The *P*-values (Prob > F) for the Cu^{2+} and Zn^{2+} models were less than 0.001, indicating that the Cu^{2+} and Zn^{2+} models were highly significant. The *P*-value for the Pb^{2+} model was 0.001, which was less than 0.05, indicating that the model was significant. The *P* values (Prob > F) for the model items A, B, C, AB, AC in the Cu^{2+} model, A, B, C, A^2, B^2, C^2 in the Zn^{2+} model, and A, B, AB, AC, BC, A^2 in the Pb^{2+} model were less than 0.05, indicating that the above model terms were significant in each model [1,29]. The closer the R^2 value is to 1, the better the fit between the calculated results and the observed results of the model. The R^2 values of the three models in this experiment were 0.9670, 0.9944, 0.9723, all very close to 1. R^2_{Adj} were 0.9473, 0.9872, 0.9367, indicating that the models could explain 94.73%, 98.72%, 93.67% of the changes in response values, respectively, and the regression models could better predict the experimental results and optimize the process parameters [31]. The AP values of the models in this experiment were 24.562, 34.144, 18.622, all greater than 4, while the coefficients of variation CV were 0.63%, 0.52%, 1.06%, all less than 10%, indicating that the models are highly accurate and stable [34,35]. In summary, RSM can better simulate the removal patterns of magnetically modified lignite for Cu^{2+}, Zn^{2+}, and Pb^{2+}, and is a meaningful model.

Table 2: Analysis of variance of regression model for removal rate of Cu^{2+}

Source	Sum of squares	d_f	Mean square	F value	*P*-value Prob > F	
Model	88.69	6	14.78	48.90	<0.0001	
A	49.01	1	49.01	162.13	<0.0001	
B	2.55	1	2.55	8.45	0.0157	Significant
C	27.60	1	27.60	91.32	<0.0001	
AB	2.15	1	2.15	7.10	0.0237	
AC	7.05	1	7.05	23.32	0.0007	
BC	0.33	1	0.33	1.09	0.3202	
Residual	3.02	10	0.30			
Lack of fit	3.02	6	0.50			
Pure error	0.000	4	0.000			
Cor total	91.71	16				
Std.Dev		0.55	R-squared			0.9670
Mean		87.85	Adj R-squared			0.9473
C.V.%		0.63	Pred R-squared			0.8332
Press		15.30	Adeq precisior			24.562

Table 3: Analysis of variance of regression model for removal rate of Zn^{2+}

Source	Sum of squares	d_f	Mean square	F value	*P*-value Prob > F	
Model	229.51	9	25.50	137.74	<0.0001	
A	187.40	1	187.40	1012.28	<0.0001	Significant
B	2.99	1	2.99	16.15	0.0051	
C	2.66	1	2.66	14.35	0.0068	

(Continued)

Table 3 (continued)

Source	Sum of squares	d_f	Mean square	F value	*P*-value Prob > F	
AB	0.72	1	0.72	3.90	0.0888	
AC	0.74	1	0.74	3.99	0.0858	
BC	0.042	1	0.042	0.23	0.6483	
A^2	27.41	1	27.41	148.03	<0.0001	
B^2	2.94	1	2.94	15.90	0.0053	
C^2	6.38	1	6.38	34.48	0.0006	
Residual	1.30	7	0.19			
Lack of fit	1.30	3	0.43			
Pure error	0.000	4	0.000			
Cor total	230.80	16				
Std.Dev		0.43	R-squared			0.9944
Mean		81.96	Adj R-squared			0.9872
C.V.%		0.52	Pred R-squared			0.9102
Press		20.73	Adeq precisior			34.144

Table 4: Analysis of variance of regression model for removal rate of Pb^{2+}

Source	Sum of squares	d_f	Mean square	F value	*P*-value Prob > F	
Model	224.93	9	24.91	27.31	0.0001	Significant
A	94.53	1	94.53	103.30	<0.0001	
B	40.95	1	40.95	44.75	0.0003	
C	2.20	1	2.20	2.41	0.1645	
AB	9.92	1	9.92	10.84	0.0132	
AC	8.41	1	8.41	9.19	0.0191	
BC	2.56	1	2.56	2.80	0.0383	
A^2	57.56	1	57.56	62.91	<0.0001	
B^2	3.82	1	3.82	4.17	0.0803	
C^2	4.84	1	4.84	5.29	0.0549	
Residual	6.41	7	0.92			
Lack of fit	5.46	3	1.82	7.68	0.0390	Significant
Pure error	0.95	4	0.24			
Cor total	231.33	16				
Std.Dev		0.96	R-squared			0.9723
Mean		90.26	Adj R-squared			0.9367
C.V.%		1.06	Pred R-squared			0.6161
Press		88.80	Adeq precisior			18.622

The removal rate of Cu^{2+} increases with increasing particle size, and the increased speed is faster when the total Fe concentration and the molar ratio of Fe^{2+} to Fe^{3+} are low. The removal rate of Cu^{2+} decreases with increasing total iron concentration and declines more rapidly at a larger particle sizes and a higher molar ratio of Fe^{2+} to Fe^{3+}. The removal rate of Cu^{2+} increases with the decrease of the molar ratio of Fe^{2+} to Fe^{3+}, and the change rate increases with the increase of total Fe concentration and particle size (Fig. 2). Combining the response surface plots, considering the response surface and ANOVA results, indicates that the AB and AC interactions are very significant and the BC is not.

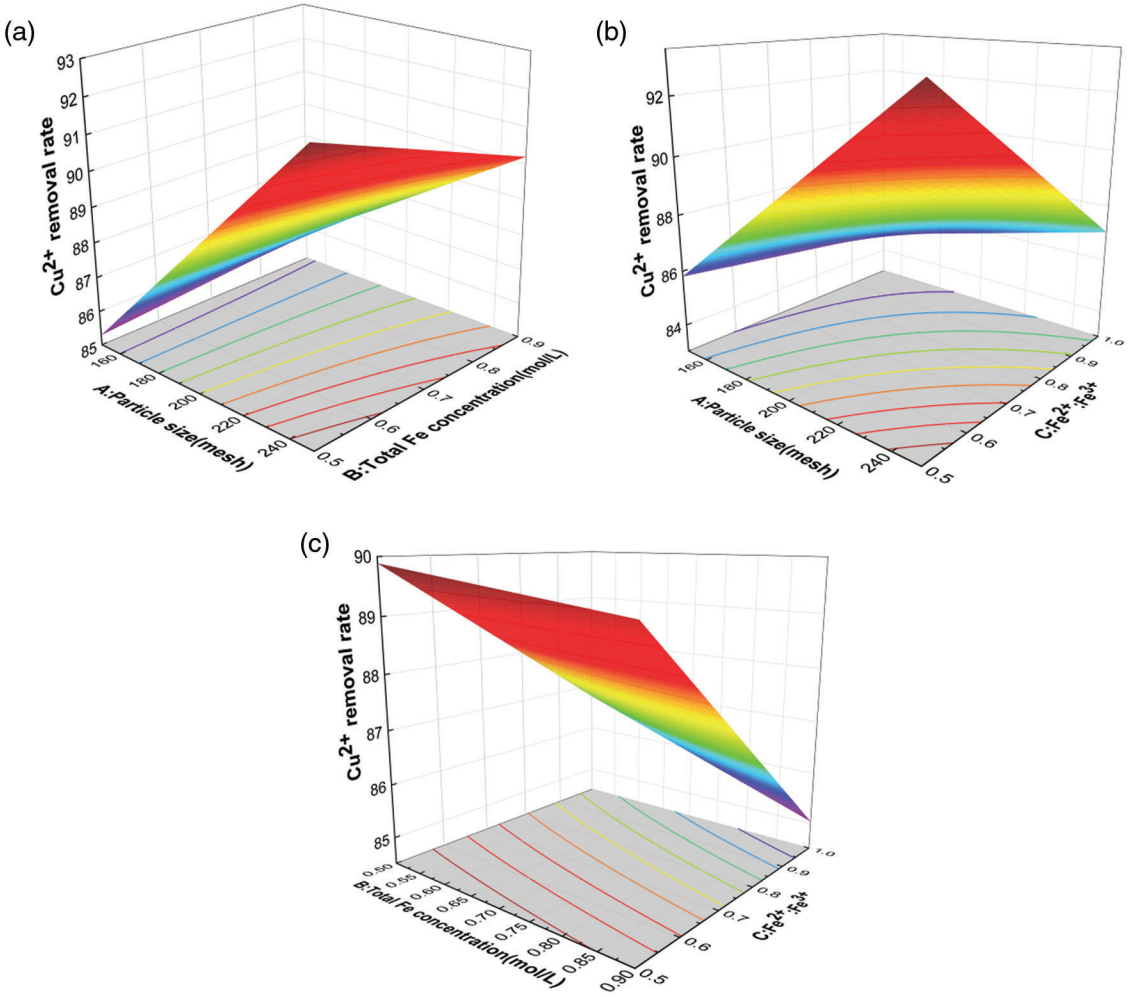

Figure 2: Response surface plot of the interaction effect of different preparation conditions on the removal rate of Cu^{2+}. (a) Particle size and total Fe concentration (b) Particle size and molar ratio of Fe^{2+} to Fe^{3+} (c) Total Fe concentration and molar ratio of Fe^{2+} to Fe^{3+}

The Zn^{2+} removal rate increases with increasing particle size, and decreases and then increases with increasing total Fe concentration and decreasing molar ratio of Fe^{2+} to Fe^{3+} (Fig. 3). The curvature of the response surface plot of AB, AC, and BC interaction is larger and the interaction effect of the binary parameters is higher, and the variance results verify this conclusion.

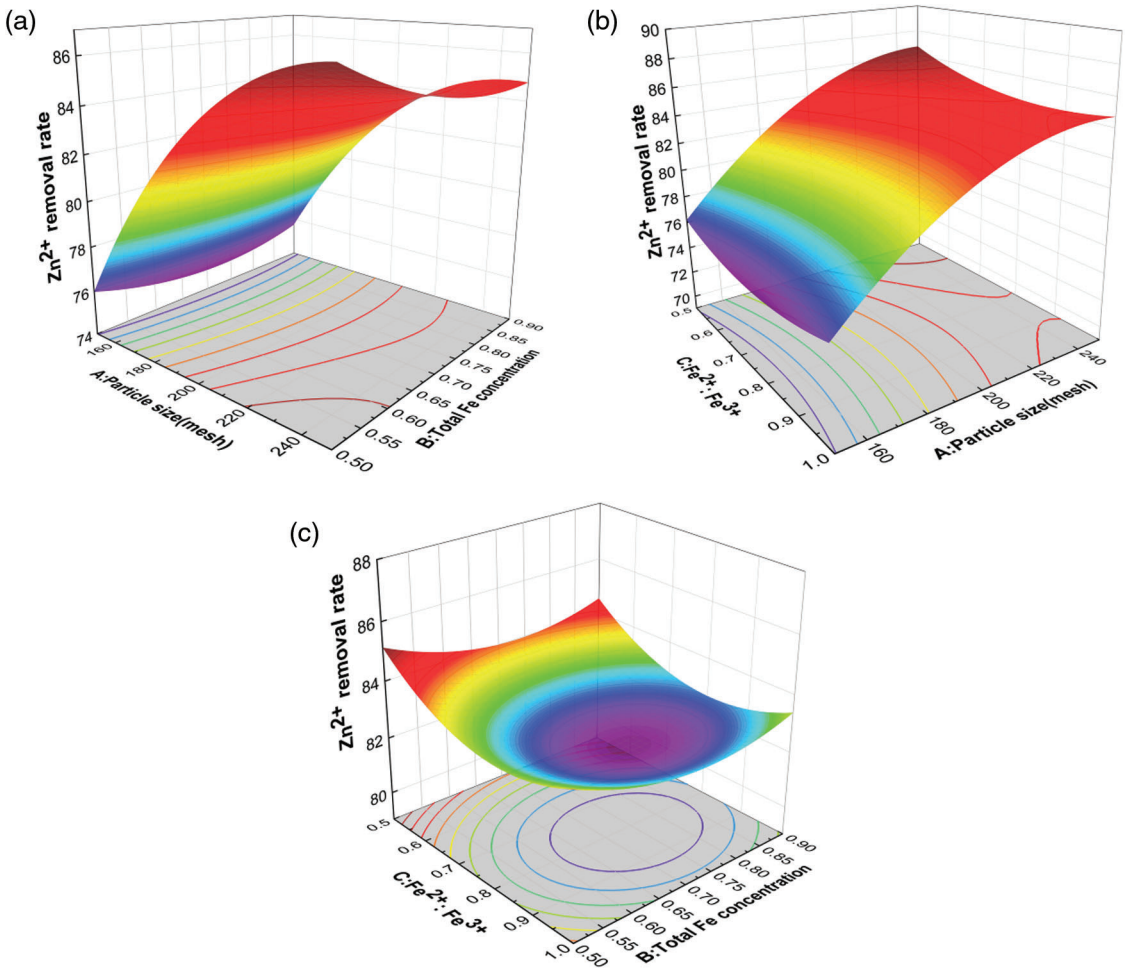

Figure 3: Response surface plot of the interaction effect of different preparation conditions on the removal rate of Zn^{2+}. (a) Particle size and total Fe concentration (b) Particle size and molar ratio of Fe^{2+} to Fe^{3+} (c) Total Fe concentration and molar ratio of Fe^{2+} to Fe^{3+}

In a certain range, the Pb^{2+} removal rate increases with the increase of particle size. When the particle size is too large, the Pb^{2+} removal rate decreases and the decrease is most obvious at the molar ratio of Fe^{2+} to Fe^{3+} of 1:1. Pb^{2+} removal rate decreases with increasing total Fe concentration, and the decrease is more obvious when the molar ratio of Fe^{2+} to Fe^{3+} is higher. When the particle size is small and the total Fe concentration is low, the Pb^{2+} removal rate decreases with the molar ratio of Fe^{2+} to Fe^{3+}, and vice versa (Fig. 4). Combined with the response surface diagram, contour diagram, and variance analysis results, the pairwise interaction of AB, AC and BC is highly significant.

The response surface BBD experimental design and the analysis of the results showed that all three factors had an effect on the ability of the prepared Fe_3O_4-L to adsorb metal ions, and there was an interactive effect between the three factors. Using the optimization function of Design Expert, the optimal preparation conditions for the preparation of Fe_3O_4-L by chemical co-precipitation were optimized as follows: the particle size of 250 mesh, the total Fe concentration of 0.5 mol/L, and the molar ratio of Fe^{2+} to Fe^{3+} of 1:2. The removal rates of Cu^{2+}, Zn^{2+}, and Pb^{2+} in AMD by Fe_3O_4-L prepared under these conditions were 94.52%, 88.49% and 96.69%.

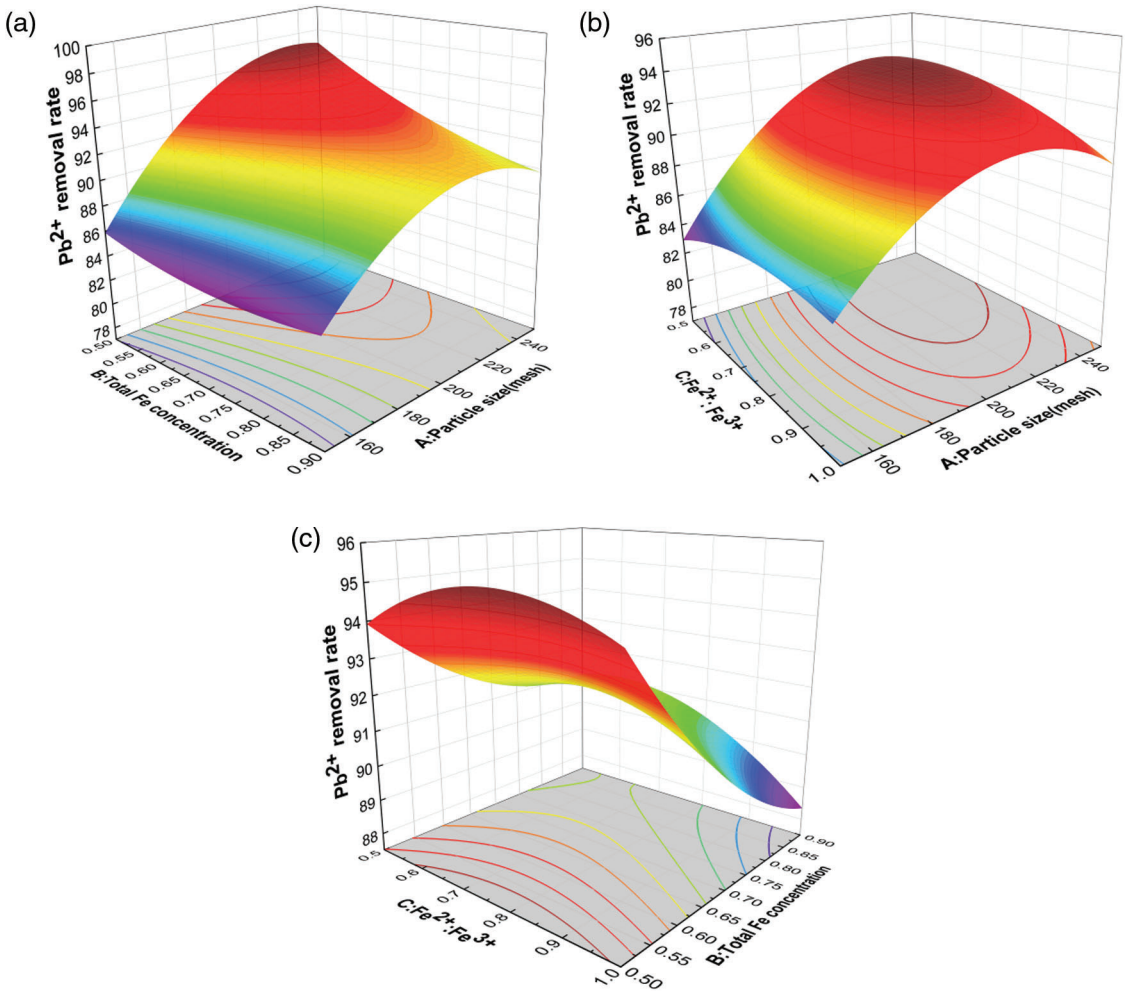

Figure 4: Response surface plot of the interaction effect of different preparation conditions on the removal rate of Pb^{2+}. (a) Particle size and total Fe concentration (b) Particle size and molar ratio of Fe^{2+} to Fe^{3+} (c) Total Fe concentration and molar ratio of Fe^{2+} to Fe^{3+}

4.3 Analysis of Adsorption Behavior

The removal of all three ions by Fe_3O_4-L shows an increasing trend as the reaction progressed. In the first 60 min, the adsorption sites on the adsorbent surface are sufficient, the mass transfer driving force between the solution and the adsorbent surface is large, and the adsorption rate increases significantly. In the middle and late stages, the adsorption sites on the surface gradually reach adsorption saturation. The adsorption of metal ions is transferred from the surface to the adsorption sites in the internal pores and the adsorption rate is slowed down. The adsorption basically reaches the equilibrium state at 180 min. The removal rates of Fe_3O_4-L for Cu^{2+}, Zn^{2+} and Pb^{2+} at equilibrium are 99.99%, 85.27% and 97.48%, respectively (Fig. 5a). Fe_3O_4-L is a porous adsorbent with a high adsorption rate loaded with Fe_3O_4 nanoparticles on the lignite matrix, which has a good prospect for the rapid removal of heavy metal cations from polluted wastewater [23,24].

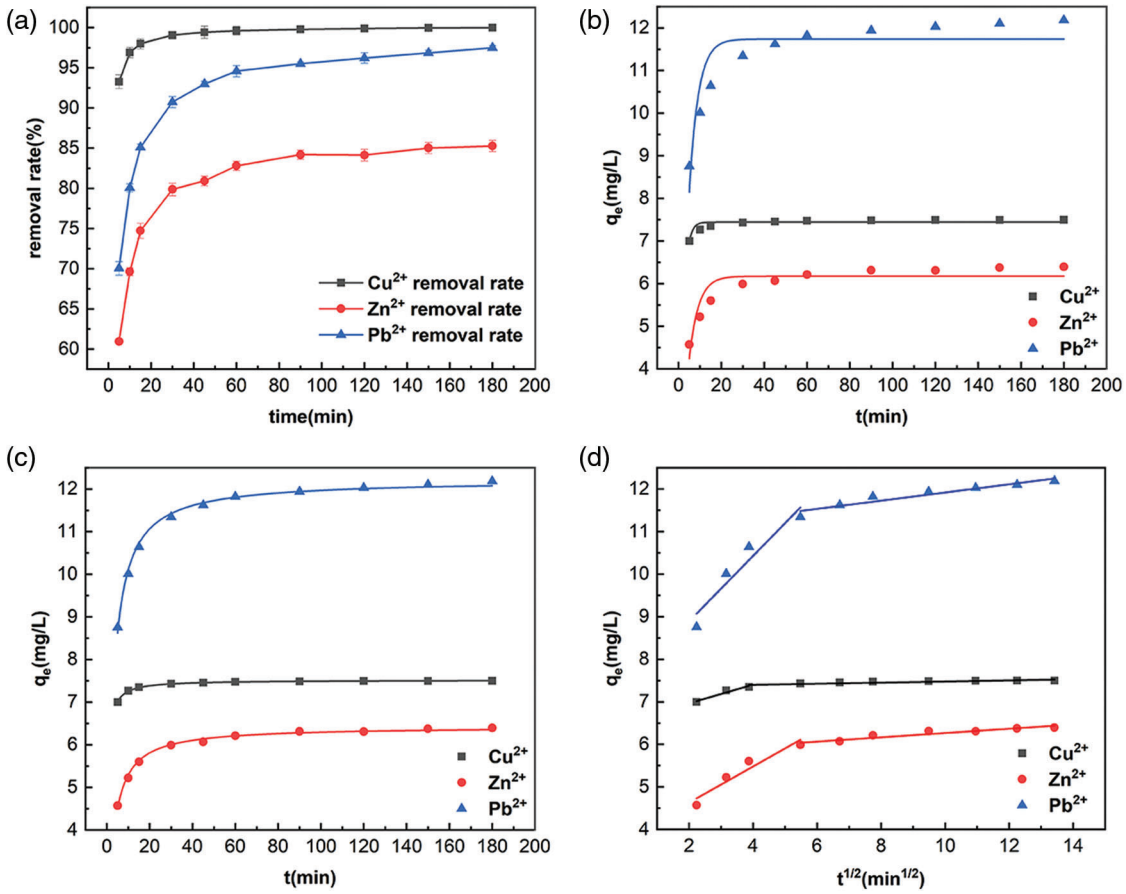

Figure 5: The effect of reaction time on the adsorption of Cu^{2+}, Zn^{2+}, Pb^{2+} by Fe_3O_4-L and the fitting results of the kinetic model. (a) The effect of reaction time on the adsorption of Cu^{2+}, Zn^{2+}, Pb^{2+} by Fe_3O_4-L (b) Fitting results of quasi-first-order kinetic model (c) Fitting results of quasi-second-order kinetic model (d) Fitting results of intra-particle diffusion model

The solute adsorption rate controls the residence time of the adsorbate at the solid-solution interface, so understanding the adsorption kinetics is important for the study of pollutant removal. In order to study the adsorption mechanism and potential rate-controlling steps throughout the adsorption process, pseudo-first-order models (such as Eq. (2)), pseudo-second-order models (such as Eq. (3)), and intraparticle diffusion models (such as Eq. (4) were utilized) to fit and analyze the kinetic process of removing Cu^{2+}, Zn^{2+}, and Pb^{2+} from Fe_3O_4-L prepared by chemical co-precipitation method. The results are shown in Table 5 and Figs. 5b–5d.

$$\ln(q_e - q_t) = \ln q_e - K_1 t \tag{2}$$

$$t/q_t = 1/(K_2 q_e^2) + t/q_e \tag{3}$$

$$q_t = K_3 \cdot t^{1/2} + C \tag{4}$$

where, q_t and q_e are the adsorption capacity at time t (min) and equilibrium, respectively (mg/g), K_1 is the rate constant of quasi-first-order kinetic reaction (min^{-1}), K_2 is the rate constant of quasi-second-order kinetic reaction (mg/g·min), K_3 is the reaction rate coefficient of intra-particle diffusion (mg/g·$min^{0.5}$), and t is the adsorption time (min) [6,36,37].

Table 5: Fitting parameters of dynamics equation

Pseudo-first-order kinetic equation	K_1(min^{-1})		q_e(mg/g)		R^2		Fit equation
Cu^{2+}	0.5535		7.7445		0.8155		$y = 7.7445*(1\text{-}e^{-0.5535x})$
Zn^{2+}	0.2323		6.1742		0.8316		$y = 6.1742*(1\text{-}e^{-0.2323x})$
Pb^{2+}	0.2357		11.7382		0.8249		$y = 11.7382*(1\text{-}e^{-0.2357x})$
Pseudo-second-order Kinetic equation	K_2(min^{-1})		q_e(mg/g)		R^2		Fit equation
Cu^{2+}	0.3644		7.5185		0.9981		$y = 20.5968x/(1 + 2.7395x)$
Zn^{2+}	0.0726		6.4299		0.9939		$y = 3.0024x/(1 + 0.4669x)$
Pb^{2+}	0.0392		12.2187		0.9947		$y = 5.8569x/(1 + 0.4793x)$
Intraparticle diffusion equation	K_{31} (min^{-1})	K_{32} (min^{-1})	C_1	C_2	R^2_1	R^2_2	Fit equation
Cu^{2+}	0.2196	0.0131	6.5258	7.3462	0.9046	0.7195	$y_1 = 0.2196x+6.5258$ $y_2 = 0.0131x+7.3462$
Zn^{2+}	0.4246	0.0504	3.7819	5.7627	0.8904	0.8878	$y_1 = 0.4246x+3.7819$ $y_2 = 0.0504x+5.7627$
Pb^{2+}	0.7692	0.0961	7.3516	10.9577	0.8778	0.8974	$y_1 = 0.7692x+7.3516$ $y_2 = 0.0961x+10.9577$

From Table 5, Figs. 5b–5d, it can be seen that the R^2 of Fe_3O_4-L adsorption process of Cu^{2+}, Zn^{2+}, Pb^{2+} fit pseudo-first-order, pseudo-second-order kinetics and intraparticle diffusion models are: 0.8155, 0.8316, 0.8249, 0.9981, 0.9939, 0.9947, 0.9046, 0.7195, 0.8904, 0.8878, 0.8778, 0.8974. The value of R^2 can be judged that the pseudo-second-order kinetic equation can better describe the adsorption process of Fe_3O_4-L to three heavy metal ions. According to the mechanism established by the pseudo-second-order kinetic equation, it can be inferred that in the process of Fe_3O_4-L adsorption of three heavy metals, physical adsorption and chemical adsorption coexist, and chemical adsorption is the main one [38,39]. All the curves of Fe_3O_4-L adsorption of Cu^{2+}, Zn^{2+}, Pb^{2+} with time can be divided into two parts, and do not pass through the coordinate origin, which indicates that the adsorption process is determined by both surface adsorption and slow channel diffusion, but the effect of diffusion adsorption on chemisorption rate Impact can be ignored [36].

In each temperature regime, an increase in the initial concentration increases the concentration difference between the solution and the adsorbent surface, leading to an increase in the adsorption of Cu^{2+}, Zn^{2+}, and Pb^{2+} per unit mass of Fe_3O_4-L (Figs. 6a, 6c, 6e). However, Fe_3O_4-L has a limited adsorption capacity and cannot further reduce the concentration of the remaining metal ions in the solution after the adsorption reaches saturation. The adsorption capacity of Fe_3O_4-L for Cu^{2+}, Zn^{2+} is larger and that for Pb^{2+} is smaller when the temperature increases, which proves that the adsorption reaction of Fe_3O_4-L for Cu^{2+} and Zn^{2+} is an absorbing reaction, and that for Pb^{2+} is an exothermic reaction. Under the same environmental conditions, the adsorption effect of Fe_3O_4-L on Cu^{2+} and Pb^{2+} was better than that of

Zn^{2+}. Differences in migration rates, ionic radii and hydration energy of Cu^{2+}, Zn^{2+} and Pb^{2+} lead to higher adsorption affinity of Fe_3O_4-L for Cu^{2+} and Pb^{2+} than for Zn^{2+} [3].

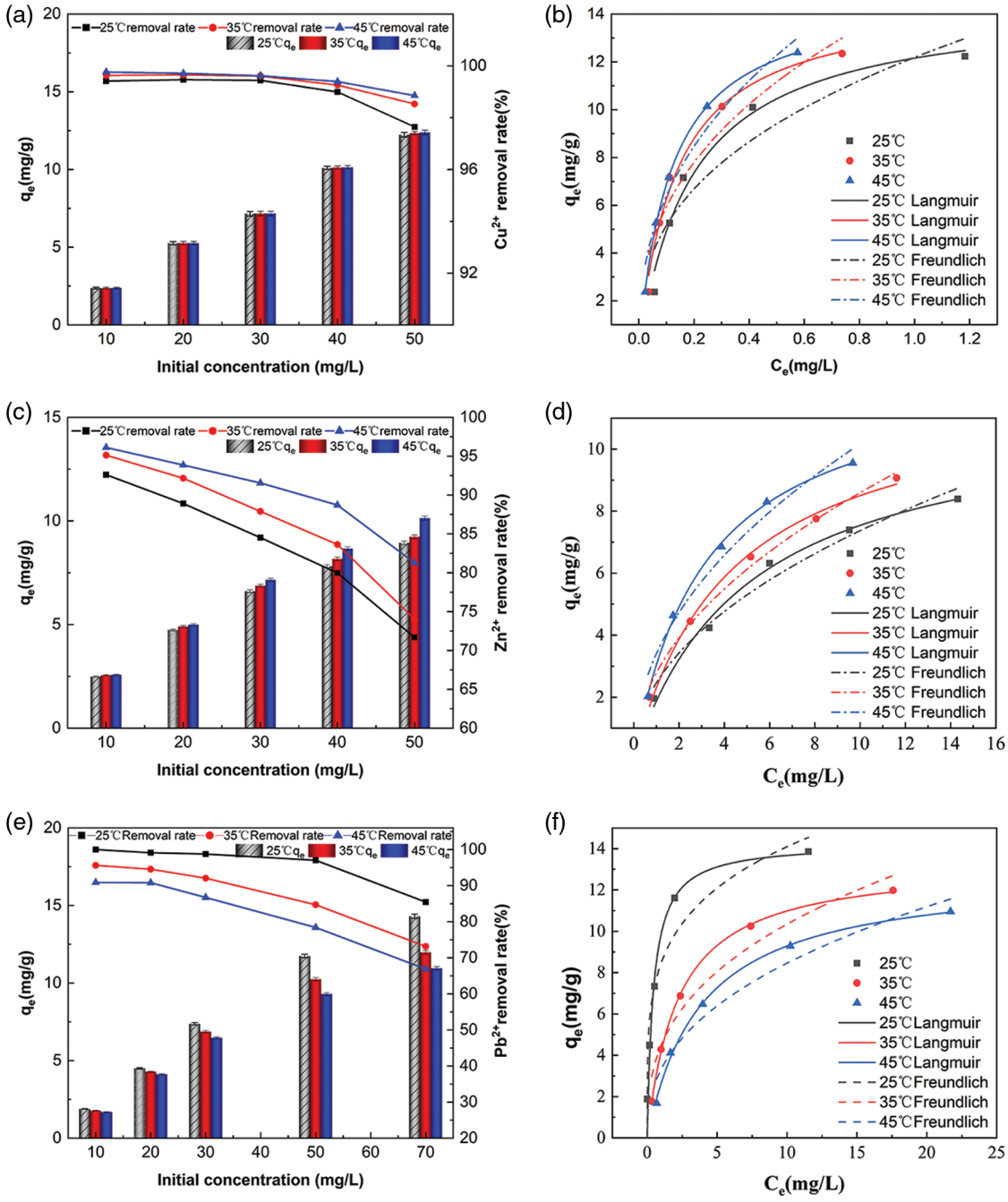

Figure 6: Effect of initial concentration on adsorption of Cu^{2+}, Zn^{2+}, Pb^{2+} by Fe_3O_4-L at different temperature systems and isotherm model fitting. (a) Effect of initial concentration on adsorption of Cu^{2+} by Fe_3O_4-L at different temperature systems. (b) Isotherm fitting of Cu^{2+} adsorbed by Fe_3O_4-L. (c) Effect of initial concentration on adsorption of Zn^{2+} by Fe_3O_4-L at different temperature systems. (d) Isotherm fitting of Zn^{2+} adsorbed by Fe_3O_4-L. (e) Effect of initial concentration on adsorption of Pb^{2+} by Fe_3O_4-L at different temperature systems (f) Isotherm fitting of Pb^{2+} adsorbed by Fe_3O_4-L

Adsorption isotherms are often used to describe the interaction of an adsorbent with an adsorbate. The Langmuir and Freundlich adsorption model are important models for describing many adsorption isotherms. Using the Langmuir and Freundlich adsorption models, the adsorption forms of Fe_3O_4-L for Cu^{2+}, Zn^{2+}, and Pb^{2+} were explored and the maximum adsorption capacity was calculated [37].

The Langmuir temperature model describes monolayer adsorption: when an adsorbent chemisorbs on a fixed number of active centers on the surface of the adsorbent, a monolayer is formed, where each active center is large enough to accommodate one adsorbed cation. All active sites are equivalent, and there is no interaction between species adsorbed on adjacent active sites. Furthermore, adsorption energy and adsorption enthalpy are equivalent. Eq. (5) represents the nonlinear form of the Langmuir isotherm:

$$q_e = \frac{K_L Q_m C_e}{C_e K_L + 1} \tag{5}$$

where, K_L is the adsorption constant related to the adsorption activation energy, the larger the value, the stronger the adsorption capacity; C_e is the remaining adsorbate concentration in the solution at equilibrium (mg/L), and q_e is the adsorption capacity at equilibrium (mg/g). Q_m is the theoretical saturation capacity of complete monolayer adsorption (mg/g), which is also related to the maximum adsorption capacity.

The Freundlich isotherm describes adsorption occurring on amorphous surfaces. This isotherm involves reversible adsorption and is not limited to monolayer formation. The Freundlich isotherm assumes that adsorption occurs at multiple locations due to the inhomogeneity of the associated surface. Eq. (6) represents the nonlinear form of Freundlich isotherm:

$$q_e = K_F C_e^{1/n} \tag{6}$$

where, K_F is the Freundlich constant related to the adsorption equilibrium, n is the Freundlich constant related to the number of active centers in the adsorbent required for the adsorption of a metal cation, and C_e (mg/L) is the remaining adsorbate concentration in the solution at equilibrium, q_e (mg/g) is the adsorption capacity at equilibrium [40].

Figs. 6b, 6d and 6f show the adsorption isotherms of Cu^{2+}, Zn^{2+}, Pb^{2+} three heavy metal ions adsorbed by Fe_3O_4-L at 25°C, 35°C and 45°C, respectively. The relevant parameters of data fitting are shown in Table 6. According to the fitting results, both Langmuir and Freundlich adsorption models can well fit the isotherm adsorption process of Fe_3O_4-L for three heavy metal ions. From the correlation coefficient R^2, the Langmuir model can better fit the adsorption process. The Langmuir isotherm is related to monolayer adsorption and homogeneous adsorption, so the adsorption of Cu^{2+}, Zn^{2+}, Pb^{2+} three heavy metal ions by Fe_3O_4-L is more inclined to homogeneous monolayer adsorption [38]. According to the Langmuir model, the theoretical maximum adsorption capacity of Fe_3O_4-L for Cu^{2+}, Zn^{2+}, and Pb^{2+} at different temperatures can be calculated, which are 14.5273 (25°C), 14.7014 (35°C), 14.9039 (45°C), 11.3407 (25°C), 12.1250 (35°C), 12.6858 (45°C), 14.2771 (25°C), 13.3843 (35°C), 12.8604 (45°C), the theoretical values are similar to the experimental results [41–43].

Table 6: Fitting parameters of Langmuir and Freundlich models for adsorption isotherms

		Langmuir model				Freundlich model		
		K_L	Q_m(mg/g)	R^2	R_L	K_F	1/n	R^2
Cu^{2+}	25°C	5.1313	14.5273	0.9725	0.004~0.0191	12.1880	0.3731	0.8556
	35°C	7.4268	14.7014	0.9829	0.003~0.0133	14.6526	0.3922	0.9224
	45°C	8.5891	14.9039	0.9996	0.002~0.0115	16.2494	0.4074	0.9385

(Continued)

Table 6 (continued)

		Langmuir model				Freundlich model		
		K_L	Q_m(mg/g)	R^2	R_L	K_F	1/n	R^2
Zn^{2+}	25°C	0.1983	11.3407	0.9917	0.092~0.335	2.4636	0.4758	0.9696
	35°C	0.2344	12.1250	0.9926	0.079~0.299	2.7848	0.4895	0.9896
	45°C	0.3155	12.6858	0.9981	0.060~0.241	3.4019	0.4754	0.9602
Pb^{2+}	25°C	2.2500	14.2771	0.9596	0.0371~1.000	8.4742	0.2210	0.8800
	35°C	0.4571	13.3843	0.9993	0.1106~0.8707	4.4872	0.3628	0.9335
	45°C	0.2599	12.8604	0.9973	0.1507~0.8505	3.3362	0.4040	0.9357

The adsorption capacity of the adsorbent is usually represented by the maximum adsorption capacity calculated by the Langmuir model. Table 7 summarizes the ability of other adsorbents reported in the literature to adsorb Cu^{2+}, Zn^{2+}, and Pb^{2+}. Obviously, Fe_3O_4-L is superior to Pellet material of iron tailings (IT) compounded with sodium alginate (SA) [44], GCM2 [45], KOH-RH [46], SiO_2/PAA [47], Sawdust of Populus alba [48] and Magnetite nanospheres [49]. Although some adsorbents such as Nanoporous activated neem bark have a better adsorption effect than Fe_3O_4-L, these adsorbents have the problems of a complicated preparation process, high cost and difficulty in recycling [41–43].

Table 7: Comparison of the adsorption capacity of Fe_3O_4-L and other adsorbents for Cu^{2+}, Zn^{2+}, Pb^{2+}

Adsorbent	Adsorption capacity (mg/g)			References
	Cu^{2+}	Zn^{2+}	Pb^{2+}	
Pellet material of iron tailings (IT) compounded with sodium alginate (SA)	2.404	1.748	10	[44]
GCM2 (A mix-ture of methylcellulose (MC), bentonite, β-zeolite and PAC)	13.3	12.59	13.684	[45]
KOH-RH (potassium hydroxide activated novel rice husk)	7.14	8.53	9.02	[46]
SiO_2/PAA	12.03	-	14.97	[47]
Sawdust of populus alba	-	8.477	10.1255	[48]
Magnetite nanospheres	-	-	13.40	[49]
Nanoporous activated neem bark	21.2	11.9	-	[41]
Zeolites from the Philippines	14.65	13.54	125.2	[42]
Utilization of biosynthesized silica-supported iron oxide nanocomposites	22.06	22.34	19.57	[43]

The stability of magnetic materials is an important factor in their adsorption applications. The results of the cyclic adsorption experiment on Fe_3O_4-L are shown in Fig. 7. It can be seen from the figure that the first removal rates of Cu^{2+}, Zn^{2+} and Pb^{2+} of Fe_3O_4-L are: 99.76%, 85.17% and 97.18%, respectively. After five cycles of adsorption-desorption experiments, the adsorption rates decreased by 6.92%, 5.84% and 4.79%,

respectively. It shows that Fe_3O_4-L has a strong regeneration ability, and has the advantages of stable recycling when treating heavy metal pollution in water [50–52].

4.4 Characterization and Mechanistic Analysis

Lignite has a dense structure and uneven shape, with many microfractures and large pores distributed on the surface. The surface of Fe_3O_4-L is rougher and covered with a large number of tiny particles (Fig. 8). The elemental composition of lignite is dominated by C, O, Al, Si and Ca, while Fe_3O_4-L adds a large amount of Fe elements compared with lignite (Fig. 9). SEM and EDS results illustrate that the Fe_3O_4-L surface was successfully loaded with a large number of Fe_3O_4 particles and had a larger specific surface area and more pore structure than lignite, which was particularly favorable for the adsorption of heavy metal ions. A large number of precipitates accumulated on the surface and pores of Fe_3O_4-L with adsorbed metal ions, and Cu, Zn and Pb elements obviously appeared on Fe_3O_4-L after adsorption, indicating that Cu^{2+}, Zn^{2+} and Pb^{2+} were successfully on Fe_3O_4-L and underwent precipitation reactions.

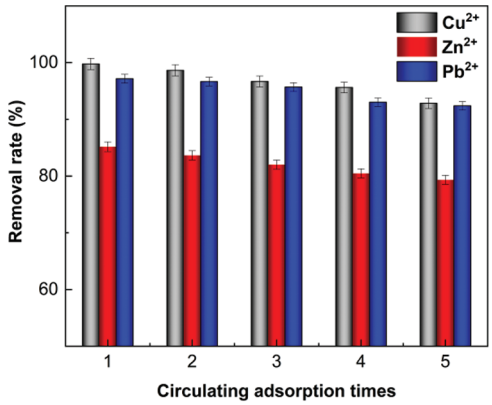

Figure 7: The experimental results of cyclic adsorption by Fe_3O_4-L

The X-ray diffraction patterns (XRD) and Fourier transform infrared spectra (FTIR) of lignite and Fe_3O_4-L before and after adsorption are shown in Fig. 10. In the figure, **a** represents lignite, **b** represents Fe_3O_4-L, and **c**, **d**, and **e** represent Fe_3O_4-L after adsorption of Cu^{2+}, Zn^{2+}, and Pb^{2+}, respectively.

Analysis of XRD results shows that lignite is mainly composed of conventional mineral components such as SiO_2, and the Fe_3O_4 crystalline phase appears obviously after magnetic modification, which confirms the successful preparation of Fe_3O_4-L. After the adsorption reaction Cu^{2+}, Zn^{2+} and Pb^{2+} existed as $CuFe_2O_4$, $Zn(OH)_2$, $ZnFe_2O_4$ and PbS and PbS, respectively, as a result of the ion exchange and complexation reaction of Cu^{2+}, Zn^{2+} and Pb^{2+} on the surface of Fe_3O_4-L. Cu^{2+}, Zn^{2+} and Pb^{2+} are adsorbed onto the Fe_3O_4-L surface driven by the mass transfer forces generated by the concentration difference between the Fe_3O_4-L surface and the solution, and precipitation occurs to form $Cu(OH)_2$, $Zn(OH)_2$, PbS. $Cu(OH)_2$, some of $Zn(OH)_2$ and $Fe(OH)_3$, the hydrolysis product of Fe^{3+}, undergo a co-precipitation reaction to form $CuFe_2O_4$ and $ZnFe_2O_4$.

Analysis of the FTIR results shows that the typical absorption peak of Fe_3O_4 clearly appears near 582 cm^{-1} in **b** compared to **a**, which is attributed to the stretching vibration of the Fe-O bond, indicating a successful preparation. Before and after the adsorption of heavy metal ions by Fe_3O_4-L, the absorption peaks near 3400, 2922, 1690, 1593 cm^{-1} were shifted and the series of absorption peaks corresponding to complex C-H out-of-plane bending vibrations were changed in the range of 600–900 cm^{-1}, which verified that the adsorption of Cu^{2+}, Zn^{2+}, and Pb^{2+} by Fe_3O_4-L was a combination of physical and chemical adsorption. Some collapse of the crystal structure of Fe_3O_4-L after adsorption of heavy metal ions occurs as a result of the reaction between metal ions and Fe-O [23,53,54].

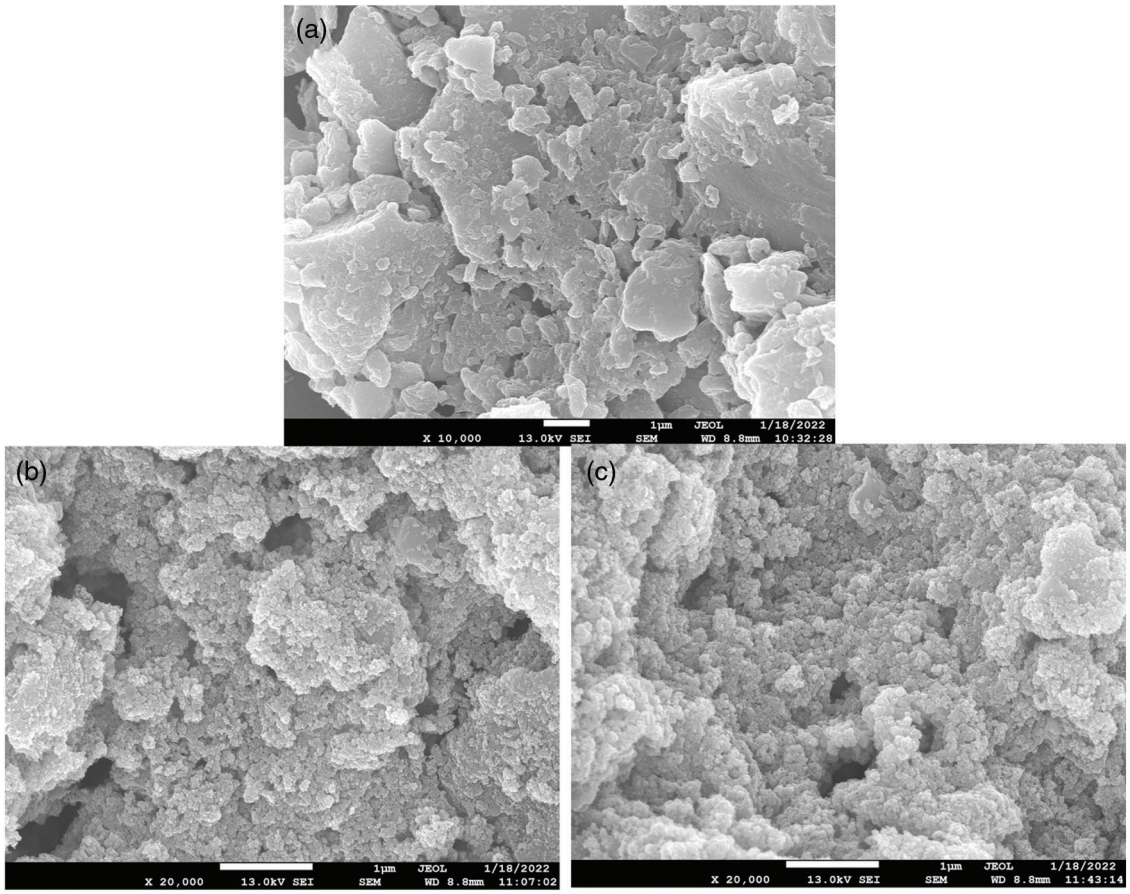

Figure 8: The SEM spectra of the materials. (a) Lignite (b) Fe_3O_4-L (c) Fe_3O_4-L after adsorption of Cu^{2+}, Zn^{2+} and Pb^{2+}

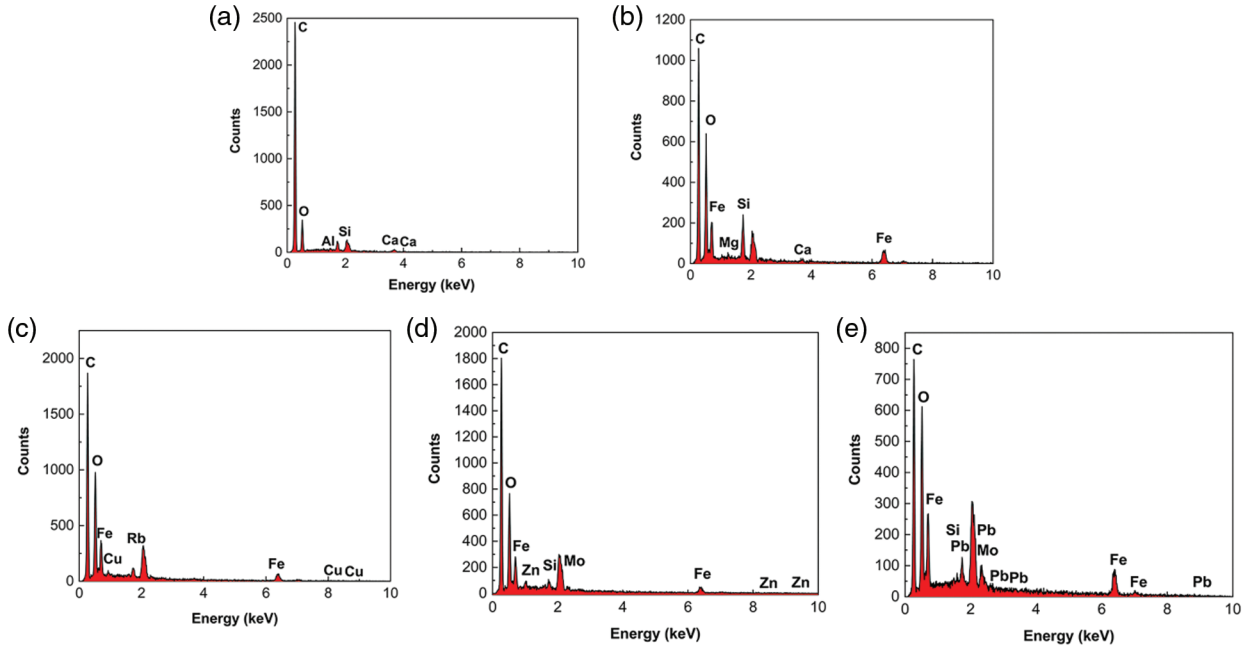

Figure 9: The EDS spectra of the materials. (a) Lignite (b) Fe_3O_4-L (c) Fe_3O_4-L after adsorption of Cu^{2+} (d) Fe_3O_4-L after adsorption of Zn^{2+} (e) Fe_3O_4-L after adsorption of Pb^{2+}

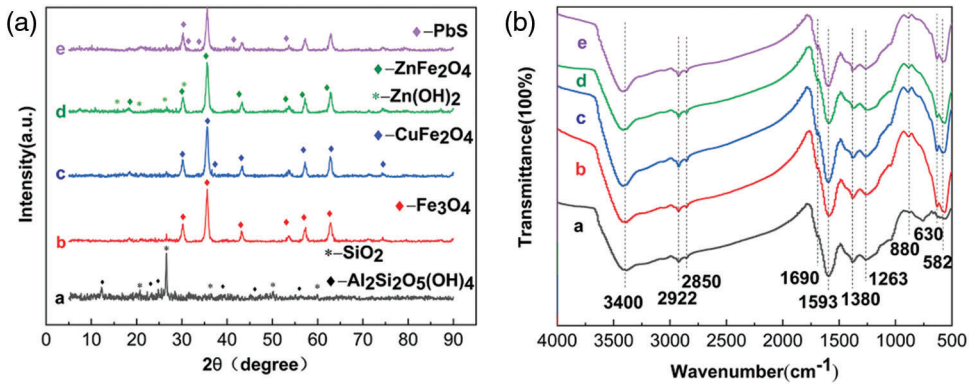

Figure 10: The XRD patterns and FTIR spectras of the materials. (a) XRD patterns (b) FTIR spectras. a. Lignite b. Fe_3O_4-L c. Fe_3O_4-L after adsorption of Cu^{2+} d. Fe_3O_4-L after adsorption of Zn^{2+} e. Fe_3O_4-L after adsorption of Pb^{2+}

5 Conclusions

(1) In the single-factor experiment for the preparation of Fe_3O_4-L by chemical co-precipitation, the particle size, the molar ratio of Fe^{2+} to Fe^{3+}, total Fe concentration and water bath temperature were used as factors to analyze the effects of Fe_3O_4-L in removing Cu^{2+}, Zn^{2+} and Pb^{2+} from AMD. It was determined that the Fe_3O_4-L prepared with a particle size of 250 mesh, a molar ratio of Fe^{2+} to Fe^{3+} of 1:2, a total Fe concentration of 0.7 mol/L, and a water bath temperature of 60°C was better. Among these reaction conditions, the particle size, the total Fe concentration, and the molar ratio of Fe^{2+} to Fe^{3+} were more influential.

(2) The response surface experiment was carried out to optimize the preparation of Fe_3O_4-L by taking the particle size, the Fe iron concentration and the molar ratio of Fe^{2+} to Fe^{3+} as factors. The results showed that the optimal reaction conditions for the preparation of Fe_3O_4-L by chemical co-precipitation were as follows: the particle size of 250 mesh, the total Fe concentration of 0.5 mol/L, and the molar ratio of Fe^{2+} to Fe^{3+} of 1:2. Under these conditions, the removal rates of Cu^{2+}, Zn^{2+} and Pb^{2+} were 94.52%, 88.49% and 96.69%, respectively.

(3) Fe_3O_4-L was prepared as adsorbent under optimal preparation conditions, and static adsorption was performed at different reaction times and different initial concentrations under different temperature systems respectively. The results showed that the adsorption of Cu^{2+}, Zn^{2+} and Pb^{2+} by Fe_3O_4-L basically reached equilibrium at 180 min, and the removal rates of Cu^{2+}, Zn^{2+} and Pb^{2+} at equilibrium were 99.99%, 85.27% and 97.48%, respectively. At the same temperature regime, an increase in the initial concentration is beneficial to enhance the adsorption capacity and efficiency, but the removal rate decreases. The adsorption reactions of Fe_3O_4-L for Cu^{2+} and Zn^{2+} are heat-absorbing reactions, and those on Pb^{2+} are exothermic reactions. Fe_3O_4-L can still maintain a high adsorption capacity after five cycles of adsorption-desorption experiments.

(4) The lignite and Fe_3O_4-L before and after adsorption were characterized by SEM-EDS, XRD and FTIR. The appearance of a large number of fine particles on the surface of lignite, a significant increase in Fe content, the appearance of the Fe_3O_4 crystalline phase and Fe-O bonding proved the success of Fe_3O_4-L preparation. Cu^{2+}, Zn^{2+} and Pb^{2+} were adsorbed by Fe_3O_4-L and mainly existed in the form of $CuFe_2O_4$, $Zn(OH)_2$, $ZnFe_2O_4$ and PbS respectively, as a result of the combined effect of physical diffusion, ion exchange and surface complexation reactions.

Acknowledgement: The authors would like to thank all editors and anonymous reviewers for their comments and suggestions.

Funding Statement: This work was supported by the National Natural Science Foundation of China (41672247), Liaoning Province's "Program for Promoting Liaoning Talents" (XLYC1807159), the Discipline Innovation Team of Liaoning Technical University (LNTU20TD-21) and the Liaoning Provincial Department of Education (LJKZ0324).

Conflicts of Interest: The authors declare that they have no conflicts of interest to report regarding the present study.

References

1. Mousavi, S. J., Parvini, M., Ghorbani, M. (2018). Adsorption of heavy metals (Cu^{2+} and Zn^{2+}) on novel bifunctional ordered mesoporous silica: Optimization by response surface methodology. *Journal of the Taiwan Institute of Chemical Engineers, 84,* 123–141. DOI 10.1016/j.jtice.2018.01.010.
2. Luptakova, A., Ubaldini, S., Macingova, E., Fornari, P., Giuliano, V. (2012). Application of physical–chemical and biological–chemical methods for heavy metals removal from acid mine drainage. *Process Biochemistry, 47(11),* 1633–1639. DOI 10.1016/j.procbio.2012.02.025.
3. Lu, X., Wang, F., Li, X. Y., Shih, K., Zeng, E. Y. (2016). Adsorption and thermal stabilization of Pb^{2+} and Cu^{2+} by zeolite. *Industrial & Engineering Chemistry Research, 55(32),* 8767–8773, 1–27. DOI 10.1021/acs.iecr.6b00896.
4. Rozumová, L., Životský, O., Seidlerová, J., Motyka, O., Šafarík, I. et al. (2016). Magnetically modified peanut husks as an effective sorbent of heavy metals. *Journal of Environmental Chemical Engineering, 4(1),* 549–555. DOI 10.1016/j.jece.2015.10.039.
5. Yin, W., Zhao, C., Xu, J., Zhang, J. (2019). The Cd(II) adsorption capacities of activated carbons optimized by RSM: Preparation and adsorption optimization. *Desalination and Water Treatment, 159,* 377–389. DOI 10.5004/dwt.2019.24185.
6. Karapinar, N., Donat, R. (2009). Adsorption behaviour of Cu^{2+} and Cd^{2+} onto natural bentonite. *Desalination, 249(1),* 123–129. DOI 10.1016/j.desal.2008.12.046.
7. Olu-Owolabi, B. I., Unuabonah, E. I. (2011). Adsorption of Zn^{2+} and Cu^{2+} onto sulphate and phosphate-modified bentonite. *Applied Clay Science, 51(1–2),* 170–173. DOI 10.1016/j.clay.2010.10.022.
8. Zhao, Y., Wang, Z., Zhao, G., Sun, R. (2019). Effects of upgrading treatment on physicochemical structure, moisture re-adsorption ability and NOx emission characteristic of lignite particles. *Energy & Fuels, 33,* 4070–4078. DOI 10.1021/acs.energyfuels.9b00306.
9. Arslan, G., Pehlivan, E. (2008). Uptake of Cr^{3+} from aqueous solution by lignite-based humic acids. *Bioresource Technology, 99(16),* 7597–7605. DOI 10.1016/j.biortech.2008.02.007.
10. Chu, H., Xue, Z., Gao, Y. (2021). Study on the adsorption behavior of mercury and arsenic by lignite. *Multipurpose Utilization of Mineral Resources, 2,* 91–96. DOI 10.3969/j.issn.1000-6532.2021.02.017.
11. Di, J., Zhang, S., Yang, Y., Liang, B., Wang, X. et al. (2020). Study on adsorption characteristics of modified lignite for Fe^{2+}, Mn^{2+} in acid mine drainage. *Coal Science and Technology.* https://kns.cnki.net/kcms/detail/11.2402.TD.20200731.1639.002.html.
12. Mohan, D., Chander, S. (2006). Removal and recovery of metal ions from acid mine drainage using lignite—A low cost sorbent. *Journal of Hazardous Materials, 137(3),* 1545–1553. DOI 10.1016/j.jhazmat.2006.04.053.
13. Peiravi, M., Mote, S. R., Mohanty, M. K., Liu, J. (2017). Bioelectrochemical treatment of acid mine drainage (AMD) from an abandoned coal mine under aerobic condition. *Journal of Hazardous Materials, 333,* 329–338. DOI 10.1016/j.jhazmat.2017.03.045.
14. Zhang, W., Zhang, B., Yuan, Z. (2012). Advances in the preparation of nanomagnetite by chemical coprecipitation. *Journal of Inner Mongolia University of Science and Technology, 31(4),* 348–350. DOI 10.16559/j.cnki.2095-2295.2012.04.015.

15. Linh, P. H., Manh, D. H., Phong, P. T., Hong, L. V., Phuc, N. X. (2014). Magnetic properties of Fe_3O_4 nanoparticles synthesized by coprecipitation method. *Journal of Superconductivity & Novel Magnetism, 27(9),* 2111–2115. DOI 10.1007/s10948-014-2561-9.
16. Wu, S., Sun, A., Zhai, F., Wang, J., Xu, W. et al. (2011). Fe_3O_4 magnetic nanoparticles synthesis from tailings by ultrasonic chemical co-precipitation. *Materials Letters, 65(12),* 1882–1884. DOI 10.1016/j.matlet.2011.03.065.
17. Mahmud, N., Nasser, M. S., El-Naas, M. H., Ba-Abbad, M. M., Mohammad, A. W. et al. (2020). Synthesis and characterization of Fe_3O_4 nanoparticles using different experimental methods. *IOP Conference Series: Materials Science and Engineering, 778,* 012028. DOI 10.1088/1757-899X/778/1/012028.
18. Safarik, I., Baldikova, E., Prochazkova, J., Safarikova, M., Pospiskova, K. (2018). Magnetically modified agricultural and food waste: Preparation and application. *Journal of Agricultural & Food Chemistry, 66(11),* 2538–2552. DOI 10.1021/acs.jafc.7b06105.
19. Lim, Y. S., Lai, C. W., Hamid, S. B. A., Julkapli, N. M., Yehya, W. A. et al. (2014). A study on growth formation of nano-sized magnetite Fe_3O_4 via co-precipitation method. *Materials Research Innovations, 18(sup6),* S6–457–S6–461. DOI 10.1179/1432891714Z.0000000001028.
20. Sebayang, P., Kurniawan, C., Aryanto, D., Setiadi, E. A., Tamba, K. et al. (2018). Preparation of Fe_3O_4/Bentonite nanocomposite from natural iron sand by co-precipitation method for adsorbents materials. *IOP Conference Series: Materials Science and Engineering, 316,* 012053. DOI 10.1088/1757-899X/316/1/012053.
21. Hashemian, S., Saffari, H., Ragabion, S. (2014). Adsorption of cobalt(II) from aqueous solutions by Fe_3O_4/Bentonite nanocomposite. *Water, Air, & Soil Pollution, 226(1),* 2212.1–2212.10. DOI 10.1007/s11270-014-2212-6.
22. Vikram, S., Dhakshnamoorthy, M., Vasanthakumari, R., Rajamani, A. R., Rangarajan, M. et al. (2015). Tuning the magnetic properties of iron oxide nanoparticles by a room-temperature air-atmosphere (RTAA) co-precipitation method. *Journal of Nanoscience & Nanotechnology, 15(5),* 3870–3878. DOI 10.1166/jnn.2015.9544.
23. Petcharoen, K., Sirivat, A. (2012). Synthesis and characterization of magnetite nanoparticles via the chemical co-precipitation method. *Materials Science & Engineering B, 177(5),* 421–427. DOI 10.1016/j.mseb.2012.01.003.
24. Meng, H., Zhang, Z., Zhao, F., Qiu, T., Yang, J. (2013). Orthogonal optimization design for preparation of Fe_3O_4 nanoparticles via chemical coprecipitation. *Applied Surface Science, 280,* 679–685. DOI 10.1016/j.apsusc.2013.05.041.
25. Dehghanpour, H. R. (2020). pH, molar ratio of ferrous to ferric ions and surfactant presence effects on physical properties of iron oxide nanoparticles generated by co-precipitation method. *Journal of Coordination Chemistry, 73(24),* 3452–3464. DOI 10.1080/00958972.2020.1849639.
26. Zhang, S., Zhang, Z., Wen, S. (2011). Nanometer ferric oxide powder was prepared by chemical coprecipitation method. *Liaoning Chemical Industry, 40(4),* 325–327 + 351. DOI 10.3969/j.issn.1004-0935.2011.04.001.
27. Wang, Z., Fu, P., Wang, R., Lui, P., Yu, Y. (2022). Study on the adsorption of Cr (VI) in water by lignite residue after humic acid extraction. *Industrial Water Treatment, 43(1),* DOI 10.19965/j.cnki.iwt.2022-0221.
28. Chou, P. I., Ng, D. Q., Li, I. C., Lin, Y. P. (2018). Effects of dissolved oxygen, pH, salinity and humic acid on the release of metal ions from PbS, CuS and ZnS during a simulated storm event. *Science of the Total Environment, 624,* 1401–1410. DOI 10.1016/j.scitotenv.2017.12.221.
29. Kumar, S. S., Bishnoi, N. R. (2017). Coagulation of landfill leachate by $FeCl_3$: Process optimization using Box–Behnken design (RSM). *Applied Water Science, 7(4),* 1943–1953. DOI 10.1007/s13201-015-0372-1.
30. Su, C., Li, W., Liu, X., Li, X. (2013). Optimal preparation conditions of sepiolite-supported nanoscale iron using response surface methodology. *Acta Scientiae Circumstantiae, 33(4),* 985–990. DOI 10.13671/j.hjkxxb.2013.04.025.
31. An, S., Li, H. (2021). Optimization of $NaHSO_3$ enhanced Fe^{2+}/persulfate system for treatment of eriochrome black T wastewater by response surface methods. *Industrial Water Treatment, 41(7),* 112–116. DOI 10.19965/j.cnki.iwt.2020-0937.
32. Huang, J., Xu, Z., Yi, C. (2007). Fe_3O_4 nanoparticles prepared by chemical co-precipitation method. *Journal of Hubei University (Natural Science), 29(1),* 50–52.

33. Zhang, S., Zhang, Z., Wen, S. (2011). Nanotriferroteoxide powder was prepared by chemical co-precipitation. *Liaoning Chemical Industry, 40(4),* 325–327.
34. Bagheri, S., Aghaei, H., Ghaedi, M., Asfaram, A., Monajemi, M. et al. (2017). Synthesis of nanocomposites of iron oxide/gold (Fe_3O_4/Au) loaded on activated carbon and their application in water treatment by using sonochemistry: Optimization study. *Ultrasonics Sonochemistry, 41,* 279–287. DOI 10.1016/j.ultsonch.2017.09.031.
35. Luo, L., Wang, G., Wang, Z., Ma, J., He, Y. et al. (2021). Optimization of fenton process on removing antibiotic resistance genes from excess sludge by single-factor experiment and response surface methodology. *Science of the Total Environment, 788,* 147889. DOI 10.1016/J.SCITOTENV.2021.147889.
36. Huang, X., Yang, J., Wang, J., Bi, J., Xie, C. et al. (2018). Design and synthesis of core–shell Fe_3O_4 @PTMT composite magnetic microspheres for adsorption of heavy metals from high salinity wastewater. *Chemosphere, 206,* 513–521. DOI 10.1016/j.chemosphere.2018.04.184.
37. Wang, S., Yu, Y., He, L., Zhang, D., Ye, M. (2019). Design of magnetic nanoparticles with high magnetic separation efficiencies and durability for Cu^{2+} adsorption. *Nanotechnology, 31(8),* 085710. DOI 10.1088/1361-6528/ab55c2.
38. Zhang, Z., Kuang, Q., Jia, X. (2010). Study on the kinetics and thermodynamics of Pb^{2+}, Cu^{2+}, Cr^{3+}, Cd^{2+}, Ni^{2+} adsorption onto peanut hull. *Ecology and Environmental Sciences, 19(12),* 2973–2977. DOI 10.16258/j.cnki.1674-5906.2010.12.018.
39. Jia, N., Wang, H., Huo, J. (2006). The study on adsorption of Zn^{2+} by modified meerschaum. *China Mining Magazine, 15(4),* 70–72.
40. Paulino, A. T., Belfiore, L. A., Kubota, L. T., Muniz, E. C., Almeida, V. C. et al. (2011). Effect of magnetite on the adsorption behavior of Pb(II), Cd(II), and Cu(II) in chitosan-based hydrogels. *Desalination, 275(1–3),* 187–196. DOI 10.1016/j.desal.2011.02.056.
41. Li, Q., Yu, J., Zhou, F., Jiang, X. (2015). Synthesis and characterization of dithiocarbamate carbon nanotubes for the removal of heavy metal ions from aqueous solutions. *Colloids and Surfaces A: Physicochemical and Engineering Aspects, 482,* 306–314. DOI 10.1016/j.colsurfa.2015.06.034.
42. Olegario, E., Pelicano, C. M., Felizco, J. C., Mendoza, H. (2019). Thermal stability and heavy metal (As^{5+}, Cu^{2+}, Ni^{2+}, Pb^{2+} and Zn^{2+}) ions uptake of the natural zeolites from the Philippines. *Materials Research Express, 6(8),* 085204. DOI 10.1088/2053-1591/ab1a73.
43. Garg, R., Garg, R., Khan, M. A., Bansal, M., Garg, V. K. (2022). Utilization of biosynthesized silica-supported iron oxide nanocomposites for the adsorptive removal of heavy metal ions from aqueous solutions. *Environmental Science and Pollution Research*. DOI 10.1007/s11356-022-21111-2.
44. Xu, C., Feng, Y., Li, H., Wu, R., Ju, J. et al. (2022). Adsorption of heavy metal ions by iron tailings: Behavior, mechanism, evaluation and new perspectives. *Journal of Cleaner Production, 344,* 131065. DOI 10.1016/j.jclepro.2022.131065.
45. Seyedein Ghannad, S. M. R., Lotfollahi, M. N. (2018). Preparation of granular composite materials as novel sorbents and their application for removal of heavy metals from solution. *International Journal of Environmental Science and Technology, 16,* 3697–3706. DOI 10.1007/s13762-018-1772-1.
46. Hossain, N., Nizamuddin, S., Shah, K. (2022). Thermal-chemical modified rice husk-based porous adsorbents for Cu(II), Pb(II), Zn(II), Mn(II) and Fe(III) adsorption. *Journal of Water Process Engineering, 46,* 102620. DOI 10.1016/j.jwpe.2022.102620.
47. Qu, J., Liao, Z., Zong, M., Zhang, F., Zhang, H. et al. (2021). Preparation of SiO_2/PAA and its adsorption behavior to Cu^{2+} and Pb^{2+}. *Industrial Water & Wastewater, 52(5),* 42–46.
48. Najam, R., Andrabi, S. M. A. (2016). Adsorption capability of sawdust of populus alba for Pb(II), Zn(II) and Cd(II) ions from aqueous solution. *Desalination and Water Treatment, 57(59),* 29019–29035. DOI 10.1080/19443994.2016.1157039.
49. Kumari, M., Pittman, C. U., Mohan, D. (2015). Heavy metals [chromium (VI) and lead (II)] removal from water using mesoporous magnetite (Fe_3O_4) nanospheres. *Journal of Colloid and Interface Science, 442,* 120–132. DOI 10.1016/j.jcis.2014.09.012.

50. Rajput, S., Pittman, C. U., Mohan, D. (2016). Magnetic magnetite (Fe_3O_4) nanoparticle synthesis and applications for lead (Pb^{2+}) and chromium (Cr^{6+}) removal from water. *Journal of Colloid and Interface Science, 468,* 334–346. DOI 10.1016/j.jcis.2015.12.008.

51. Chao, L., Wang, Y., Chen, S., Li, Y. (2021). Preparation and adsorption properties of chitosan-modified magnetic nanoparticles for removal of Mo (VI) ions. *Polish Journal of Environmental Studies, 30(3),* 2489–2498. DOI 10.15244/pjoes/130039.

52. Zhu, C., Dong, X., Chen, Z., Naidu, R. (2016). Adsorption of aqueous Pb(II), Cu(II), Zn(II) ions by amorphous tin(VI) hydrogen phosphate: An excellent inorganic adsorbent. *International Journal of Environmental Science and Technology, 13(5),* 1257–1268. DOI 10.1007/s13762-016-0964-9.

53. Ren, Y., Abbood, H. A., He, F., Peng, H., Huang, K. (2013). Magnetic EDTA-modified chitosan/SiO_2/Fe_3O_4 adsorbent: Preparation, characterization, and application in heavy metal adsorption. *Chemical Engineering Journal, 226,* 300–311. DOI 10.1016/j.cej.2013.04.059.

54. Di, J., Li, M., Wang, X., Yang, Y., Liang, B. et al. (2020). Experimental study on adsorption of Cu^{2+} and Zn^{2+} in acid mine drainage by modified lignite. *Coal Science and Technology, 50(3),* 301–307.